Journal of Materials Chemistry C

Accepted Manuscript

This article can be cited before page numbers have been issued, to do this please use: J. Jou, S. Sahoo, S. Kumar, H. Yu, P. Fang, M. Singh, G. Krucaite, D. Y. Volyniuk, J. V. Grazulevicius and S. Grigalevicius, *J. Mater. Chem. C*, 2015, DOI: 10.1039/C5TC02889B.

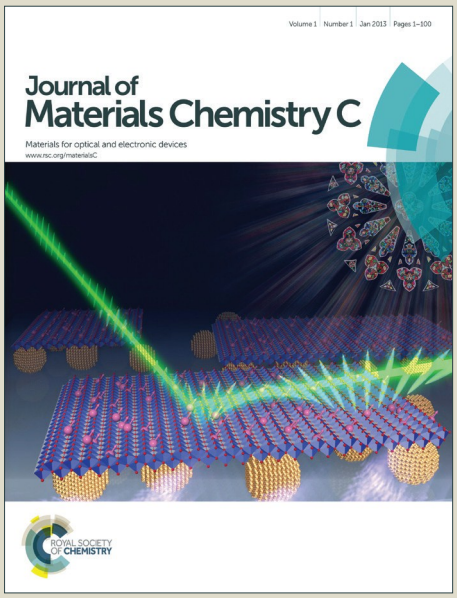

ROYAL SOCIETY OF CHEMISTRY

www.rsc.org/materialsC

View Article Online
DOI: 10.1039/C5TC02889B

Wet- and dry-process feasible carbazole type host for highly efficient phosphorescent OLEDs

Jwo-Huei Jou[a,*], Snehasis Sahoo[a], Sudhir Kumar[a,b], Hui-Huan Yu[a], Po-Hsun Fang[a], Meenu Singh[a], Gintare Krucaite[c], Dmytro Volyniuk[c], Juozas Vidas Grazulevicius[c], Saulius Grigalevicius[c,*]

[a]Department of Materials Science and Engineering, National Tsing-Hua University, Hsin-Chu-30013, Taiwan, Republic of China.
[b]Institute for Chemical and Bioengineering, ETH Zürich, Vladimir Prelog Web 1, 8093 Zürich, Switzerland.
[c]Department of Polymer Chemistry and Technology, Kaunas University of Technology, Radvilenu plentas 19, LT50254, Kaunas, Lithuania.

*Corresponding authors: jjou@mx.nthu.edu.tw (J.-H. Jou) and saulius.grigalevicius@ktu.lt (S. Grigalevicius)

Abstract

A wet- and dry-process feasible host material is crucial to realize, respectively, low cost roll-to-roll fabrication of large area and high performance organic light-emitting diodes (OLEDs) with precise deposition of organic layers. We demonstrate in this study, high efficiency phosphorescent OLED devices by employing a newly synthesized carbazole based host material 1,6-bis[3-(2-methoxy-3-pyridinyl)carbazol-9-yl]hexane (compound **5**). Moreover, two other carbazole hosts 1,6-bis[3-(6-methoxy-3-pyridinyl)carbazol-9-yl]hexane (compound **4**) and 3,6-di(2-methoxy-3-pyridinyl)-9-ethylcarbazole (compound **6**) are also synthesized for comparison. By doping a typical green emitter *fac* tris(2-phenylpyridine)iridium ($Ir(ppy)_3$) in the compound **5**, for example, the resultant wet-processed device exhibits at 100 cd m^{-2} a current efficiency

View Article Online
DOI: 10.1039/C5TC02889B

of 27 cd A^{-1} and a power efficiency of 16.1 lm W^{-1}. The dry-processed device shows a current efficiency of 61 cd A^{-1} and a power efficiency of 62.8 lm W^{-1}. The high efficiency may be attributed to the host possessing an effective host-to-guest energy transfer, effective carrier injection balance, and the device architecture enabling excitons to generate on both host and guest.

1. Introduction

Organic light-emitting diodes (OLEDs) have drawn enormous attention due to their increasing applications in flat-panel displays and solid state lightings.[1] A wide variety of OLED based display devices have already emerged in the market from the last few years, and lighting products are also developing rapidly.[1-2] Nowadays, phosphorescent materials become ideal for fabricating high-efficiency OLEDs, because they can theoretically approach a nearly 100% internal quantum efficiency by harvesting singlet and triplet excitons simultaneously through intersystem crossing.[3-6] A suitable phosphorescent host material can play an effective role in reducing both the concentration quenching and triplet-triplet annihilation effects frequently occurring in an undoped system.[7] The host materials should have a few important properties, such as an energy level matching with the neighboring layers to ensure a low injection barrier, a good carrier mobility to realize a high recombination rate, a proper bipolarity to maximize charge injection balance, an effective host-to-guest energy transfer,[8-9] and a

View Article Online
DOI: 10.1039/C5TC02889B

high triplet energy to avoid back energy transfer.[10] In addition, a good host material is expected to have a high glass transition temperature (T_g) to realize high thermal and morphological stability of the device.[11-13]

OLED devices can be fabricated by utilizing both thermal evaporation and spin-coating processes. It would be ideal if a host material possesses both wet- and dry-process feasibilities so that it can realize low cost roll-to-roll fabrication for large area-size devices and high brightness as well as long lifetime for high performance devices, respectively.[14-19]

In the past years, a few wet- and dry-processable molecular host materials had been reported. For example, Jou's group reported a wet- and dry-process feasible EML system containing a 4,4'-bis(carbazol-9-yl)biphenyl as host and a bis[5-methyl-8-trifl uorome-thyl-5*H*-benzo(c)(1,5)naphthyridin-6-one] iridium (acetylacetonate) ((2-CF_3BNO)$_2$ Ir(acac)) as green light emitting guest. The device showed, at 100 cd m^{-2}, an efficacy of 78.6 lm W^{-1} via spin-coating, while 65.4 lm W^{-1} via vapor deposition.[17] They further reported an efficacy of 47.1 lm W^{-1} via solution process, and 60.6 lm W^{-1} via thermal evaporation process, by using a 4,4',4"-tri(*N*-carbazolyl)triphenylamine (TCTA) as host and a bis[5-methyl-5*H*-benzo[c][1,5] naphthyridin-6-one]iridium (picolinate) (BNO) as green emitter.[18] Lin's group achieved an efficacy of 70 lm W^{-1} via solution process, and 21 lm W^{-1} via thermal evaporation process, by using a 4-4'-

View Article Online
DOI: 10.1039/C5TC02889B

bis(carbazol-9-yl)biphenyl (CBP) as host and a bis[5-methyl-7-trifluoromethyl-5*H*-benzo(c) (1,5) naphthyridin-6-one]iridium(picolinate) ($(CF_3BNO)_2IrPLA$) as green emitter.[19]

In this study, we present a newly synthesized carbazole-type host material 1,6-bis[3-(2-methoxy-3-pyridinyl)carbazol-9-yl]hexane **(5)** that possesses a high triplet energy and is wet- and dry-process feasible. Two other carbazole group based hosts, 1,6-bis[3-(6-methoxy-3-pyridinyl)carbazol-9-yl]hexane **(4)** and 3,6-di(2-methoxy-3-pyridinyl)-9-ethylcarbazole **(6)**, were also synthesized for comparison. By spin coating, at 100 cd m^{-2} for example, the host **5** containing device shows an efficacy of 16.1 lm W^{-1} and a current efficiency of 27 cd A^{-1}, while the host **4** and **6** containing devices show an efficacy of 12 lm W^{-1} with a current efficiency of 21.4 cd A^{-1} and 2.4 lm W^{-1} with 3.4 cd A^{-1}. By using dry-process, the host **5** composing device doped with an $Ir(ppy)_3$ green emitter shows an efficacy of 62.8 lm W^{-1} and current efficiency of 61 cd A^{-1}, while compound **4** and compound **6** containing devices exhibits an efficacy of 42.9 lm W^{-1} with 41.8 cd A^{-1} and 7.9 lm W^{-1} with 9.5 cd A^{-1}, respectively.

2. Results and discussion

2.1. *Synthesis*

As shown in **Scheme 1**, the synthesis of the methoxypyridinyl substituted carbazole based host materials, **4-6**, were carried out by Suzuki coupling reaction. The host

View Article Online
DOI: 10.1039/C5TC02889B

materials **4** and **5** were synthesized by coupling reaction of a 1,6-bis(3-iodocarbazol-9-yl)hexane (**3**) with an excess of a 6-methoxy-3-pyridinylboronic acid and a 2-methoxy-3-pyridinylboronic acid, respectively. Moreover, the host **6** was synthesized by coupling reaction of a 3,6-di-iodo-9-ethylcarbazole (DECr)[20] with an excess amount of a 2-methoxy-3-pyridinylboronic acid. The key material, i.e. 3-iodo-9*H*-carbazole (**2**), was synthesized from a commercially available 9*H*-carbazole using Tucker iodination reaction.[21] The twin-derivative **3** that contains two 3-iodocarbazol-9-yl fragments was synthesized by the reaction of a 1,6-dibromohexane with an excess of the 3-iodo-derivative of compound **2** under basic conditions by using the prior reaction procedure.[22] The resultant compounds (**2-6**) were characterized by using ^{1}H NMR, ^{13}CNMR spectroscopies and mass spectrometry. The ^{1}H NMR and ^{13}C NMR spectra of compounds **4**, **5** and **6** were presented in the Figure S1 and Figure S2. The data were found in good agreement with the proposed structures.

View Article Online
DOI: 10.1039/C5TC02889B

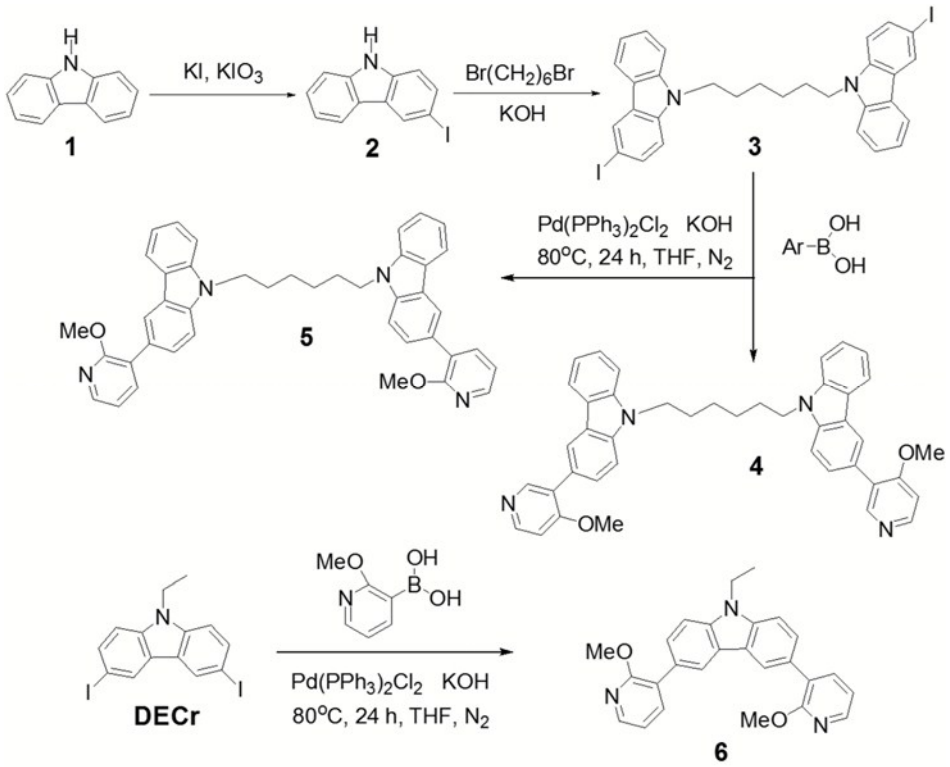

Scheme 1. Schematic illustration of the synthesis of the carbazole-type hosts **4**, **5**, and **6**.

Table 1. Thermal, photophysical, and electrochemical characteristics of the novel host **5**, compared with those of the other two molecular hosts **4** and **6**.

Host	T_g[a] [°C]	T_m[b] [°C]	T_d[c] [°C]	Hole mobility ($cm^2V^{-1}s^{-1}$)	HOMO[d] [eV]	LUMO[e] [eV]	E_g[f] [eV]	λ_{abs} [nm]	λ_{PL}[g] [nm]	λ_{PL}[h] [nm]	E_T[i] [eV]
4	51	167	409	2×10^{-4}	5.60	2.26	3.34	283	391, 375	483, 455	2.56
5	54	-	402	4×10^{-4}	5.24	1.91	3.33	283	391, 374	483, 455	2.56
6	57	137	353	5×10^{-4}	5.71	2.31	3.40	302	385	501	2.47

[a]Glass transition temperature, [b]melting temperature, [c]decomposition temperature, [d]HOMO values are measured by the cyclic voltammetry (CV) method. The semi-oxidation potential ($E^{ox}_{1/2}$) was calculated from (E_{p1} + E_{p2})/2 -0.48, where 0.48 is the correction value obtained by the oxidation system added to ferrocenium/ferrocene (F_c^+/F_c) as the internal standard, and then the energy of HOMO could be obtained from the E_{HOMO} = -($E^{ox}_{1/2}$ + 5.1).[23] [e]The energy of LUMO could be obtained by subtracting the optical bandgap from the HOMO energy level, [E_{LUMO} = (E_{HOMO} -E_g)], [f]optical bandgap, [g]PL spectra at room temperature, [h]PL spectra at 77K, and [i]triplet energy of hosts.

View Article Online
DOI: 10.1039/C5TC02889B

2.2 Carrier mobility measurement

The hole mobility (μ_h) of the host materials (**4-6**) was characterized by the time-of-flight (TOF) technique.[24, 25] The μ_h was calculated by the formula of $\mu_h = d^2/(V.t_T)$, where d is the layer thickness of the hosts (**4-6**), V the applied voltage, and t_T the transit time.[26, 27] (see Fig. S3 for detail double logarithmic plots) The μ_h determined for compounds **4-6** is shown as a function of the square root of electric field ($E_{1/2}$) in **Fig. 1**. The μ_h of hosts **4-6** ranges from 5×10^{-4} to 2×10^{-4} $cm^2/(V\cdot s)$, as shown in **Table 1**. However, no detectable electron mobility (μ_e) can be observed for the newly synthesized host materials **4-6** by the TOF method.

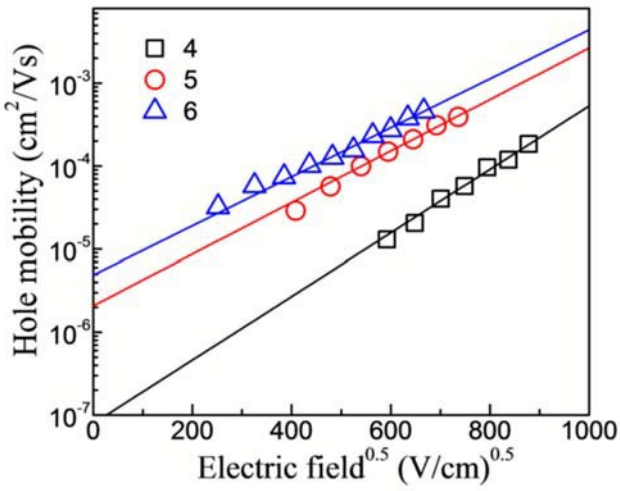

Figure 1. Hole mobilities of the hosts, **4**, **5**, and **6**, as a function of square root of electric field.

The compounds **4**, **5**, and **6** show hole mobility in the order **4**<**5**<**6**. The reason why compound **5** and compound **6** show a higher hole mobility than that of compound **4** counterpart may be attributed to the position of methoxy group on the pyridine unit. The 6-methoxyl-3-pyridinyl substituted compound **4** with a para-linked methoxy group

View Article Online
DOI: 10.1039/C5TC02889B

showed the lowest hole mobility because a large number of electrons are delocalized near the N-atom. On the other hand, the 2-methoxyl-3-pyridinyl substituted compound **5** and compound **6** show high hole mobility due to the ortho-linked electron donating methoxy group, resulting into the localization of electrons near the N-atom. Amongst, compound 6 shows a highest hole mobility because of the extended conjugation in the molecule, while the conjugation is disrupted in compound 5 due to the long alkyl chain that connected the two carbazole units.[28]

2.3. *Thermal characteristics*

The thermal characteristics of compounds **4-6** were characterized by using differential scanning calorimetry (DSC) and thermogravimetric analysis (TGA) techniques. As shown in **Table 1**, the compound **4** shows a 5% weight loss decomposition temperature (T_d) of 409 ^oC, while 402 ^oC and 353 ^oC for the **5** and **6** counterparts, respectively. The reason why the compounds **4** and **5** show higher thermal stability than that of the compound **6** because of their higher molecular weight, which is resulted due to the twin-carbazole molecular structures. The melting temperatures (T_m) of the hosts **4-6** range from 137 ^oC to 167 ^oC, while the glass transition temperatures (T_g) range from 51 ^oC to 57 ^oC. The reason why single carbazole unit based compound **6** shows a slightly higher T_g (57 ^oC) than that of twin carbazole based counterparts because of their normal hexane linkage.

View Article Online
DOI: 10.1039/C5TC02889B

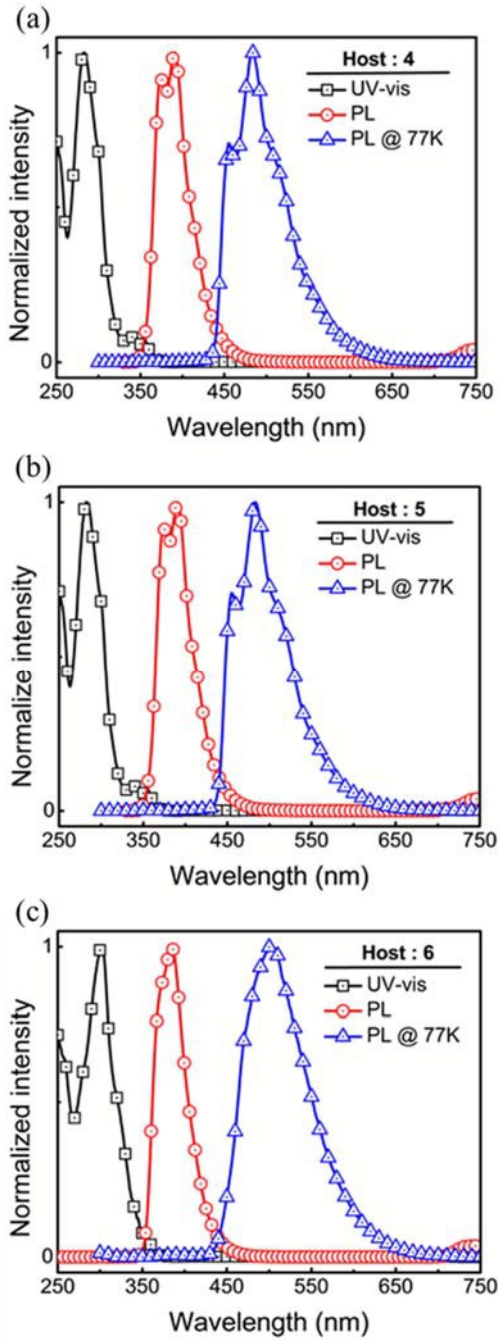

Figure 2. Ultraviolet-visible, photoluminescence and phosphorescence (PL at 77K) spectra of the novel carbazole-type compounds, (a) **4**, (b) **5**, and (c) **6**. All the data were measured in tetrahydrofuran.

2.4. *Photophysical and electrochemical characteristics*

As shown in **Fig. 2**, the ultraviolet–visible (UV–Vis) and photoluminescence (PL)

View Article Online
DOI: 10.1039/C5TC02889B

spectra of the compounds **4**, **5**, and **6** were measured in tetrahydrofuran (THF) at room temperature. The optical band gaps were estimated from the edge of the absorption spectra, giving values of 3.34, 3.33, and 3.40 for the compounds **4**, **5**, and **6**, respectively. The triplet-energies were calculated from the first triplet emission peak of the low temperature PL spectrum measured in cryogenic medium (liquid N_2) at 77K. The compounds **4** and **5** showed a triplet-energy, 2.56 eV, whereas, the compound **6** showed a slightly lower triplet energy of 2.47 eV. The reason why host-**6** shows a lower triplet energy may be attributed to its extended conjugation in molecular structure, while in host-**5** conjugation is interrupted by a long aliphatic chain. As reported by Woon et al., the triplet energy would decrease with the increase in effective conjugation length.[29] Moreover, the host **4** and **5** shows a clear vibronic band at 355 nm due to the dimer structure. The reason why a vibronic band does not appear in the low temperature (at 77K) PL spectrum of host **6** is because of the absence of dimer.[30]

The electrochemical properties of the three carbazole-type host molecules 4–6 were measured by cyclic voltammetry (CV). The highest occupied molecular orbital (HOMO) energy levels of the hosts were estimated to be 5.60 eV, 5.24 eV, and 5.71 eV for the compounds **4**, **5**, and **6**, respectively, using oxidation potential. The lowest unoccupied molecular orbital (LUMO) energy levels were calculated to be 2.26 eV, 1.91 eV, and 2.31 eV for the compounds **4**, **5**, and **6**, respectively, from HOMO energy levels and optical energy band gaps, which were estimated from the edge of the absorption spectra (**Table 1**).

2.5. *Electroluminescence properties of devices*

View Article Online
DOI: 10.1039/C5TC02889B

Fig. 3 illustrates the schematic energy-level diagram of green OLED devices containing newly synthesized host materials **4**, **5**, and **6** and green emitter $Ir(ppy)_3$.The devices were composed of a 125 nm indium tin oxide (ITO) anode layer, followed by a 35 nm poly(3,4-ethylene-dioxythiophene)-poly(styrenesulfonate) (PEDOT:PSS) hole injection layer (HIL), **Fig. 3 (a)** a 20 nm single emissive layer (EML) with the green emitter ($Ir(ppy)_3$) doped in the host **5** via spin-coating deposition (wet-process) and physical vapor deposition (dry-process), **Fig. 3 (b)** a 20 nm di-[4-(*N,N*-ditolyl-amino)-phenyl]cyclohexane (TAPC) hole transporting layer (HTL) was also thermally deposited between the PEDOT:PSS and EML of dry-processed device, a 32 nm 1,3,5-tris(*N*-phenylbenzimidazol-2-yl)benzene (TPBi) electron transporting layer (ETL), a 1 nm lithium fluoride (LiF) layer, and a 100 nm aluminum (Al) cathode layer. Besides the host **5**, two other hosts, **4** and **6** were also studied herein.

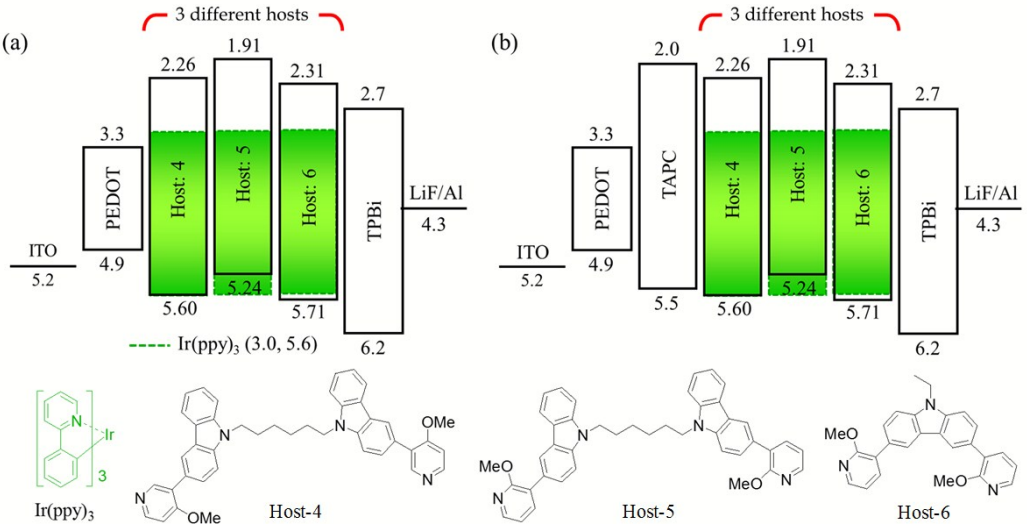

Figure 3. Schematic diagrams of the energy levels of the OLED devices, containing a green emitter $Ir(ppy)_3$ in the three different hosts: **4**, **5**, and **6**, using (a) wet- and dry-

View Article Online
DOI: 10.1039/C5TC02889B

processes, and (b) dry-process with the incorporation of an hole transporting layer (HTL) TAPC. Molecular structures of the typical green emitter and the three newly synthesized hosts were also presented.

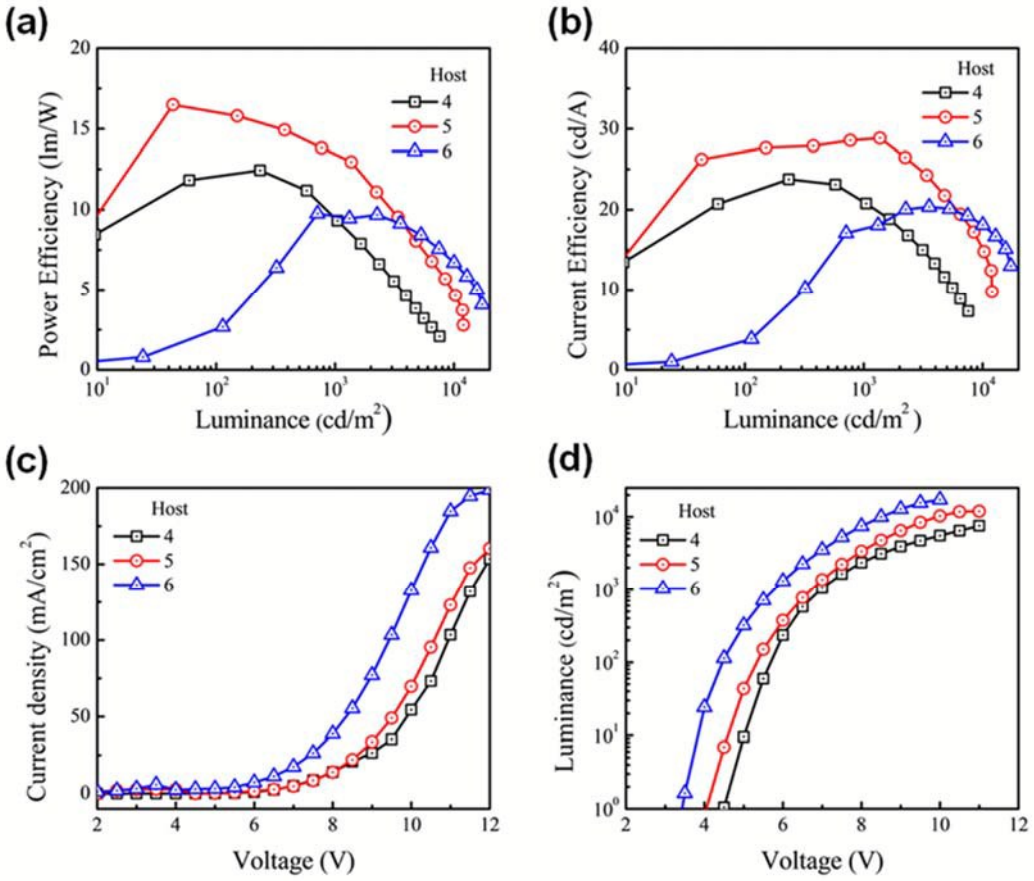

Figure 4. Comparison of a) power efficiency, b) current efficiency, c) current density, and d) luminance of the devices with a 15 wt% ratio $Ir(ppy)_3$ doped in the hosts **4**, **5**, and **6**.

Table 2: Effects of doping concentrations of $Ir(ppy)_3$ on the operation voltage (OV), power efficiency (η_p), current efficiency (η_c), external quantum efficiency (η_{ext}), CIE coordinates, and maximum luminance of the novel host materials, **4**, **5**, and **6** containing wet-processed OLED devices.

Host	Dopant (wt%)	V_{ON} (V)	OV (V)	PE (lm/W)	CE (cd/A)	EQE (%)	CIE coordinates	Max. Luminance (cd/m^2)
		@ 10 cd/m^2			@ 100/1000 cd/m^2			
4	10	4.6	5.5/ 7.4	3.5/ 6.4	6.2/ 15.0	1.7/ 4.2	(0.31, 0.62)/ (0.31, 0.62)	5313
	12.5	5.0	5.6/ 6.9	9.0/ 7.9	16.0/ 17.4	4.4/ 4.8	(0.31, 0.63)/ (0.31, 0.63)	7024
	15	5.0	5.6/ 6.9	12.0/ 9.5	21.4/ 21.0	5.9/ 5.8	(0.31, 0.62)/ (0.31, 0.62)	7575
	17.5	5.0	5.6/ 6.7	9.1/ 9.2	16.2/ 19.7	4.5/ 5.4	(0.32, 0.62)/ (0.32, 0.62)	7733
5	10	4.4	5.2/ 6.7	13.1/ 10.3	21.5/ 21.9	6.0/ 6.1	(0.31, 0.62)/ (0.31, 0.62)	10340
	12.5	4.5	4.9/ 6.2	14.2/ 13.5	22.6/ 26.6	6.3/ 7.4	(0.31, 0.62)/ (0.31, 0.62)	11240
	15	4.5	5.3/ 6.7	16.1/ 13.5	27.0/ 28.7	7.5/ 8.0	(0.32, 0.62)/ (0.32, 0.62)	12000
	17.5	4.6	4.7/ 6.1	11.3/ 13.4	17.3/ 26.0	4.7/ 7.1	(0.31, 0.63)/ (0.31, 0.63)	12910
6	10	4.0	4.7/ 6.3	3.4/ 8.1	5.2/ 16.2	1.5/ 4.6	(0.31, 0.62)/ (0.31, 0.62)	12990
	12.5	3.7	4.4/ 5.7	4.5/ 11.6	6.4/ 21.0	1.8/ 5.8	(0.31, 0.63)/ (0.31, 0.63)	17230
	15	3.7	4.4/ 5.7	2.4/ 9.6	3.4/ 17.6	0.9/ 4.8	(0.31, 0.63)/ (0.31, 0.63)	17260
	17.5	3.7	4.3/ 5.5	3.1/ 11.9	4.4/ 20.9	1.2/ 5.8	(0.31, 0.62)/ (0.31, 0.62)	16990

View Article Online
DOI: 10.1039/C5TC02889B

2.5.1 *Wet-processed devices*

Table 2 shows the electroluminescent characteristics of the host **5** based wet-processed green OLED compared with those of the host **4** and **6** containing counterparts. As shown in **Fig. 4**, the host **5**-containing device exhibited a power efficiency of 16.1 lm W^{-1} with a current efficiency of 27 cd A^{-1} at 100 cd m^{-2}. For the host **4** containing device, its power efficiency was 12 lm W^{-1} (21.4 cd A^{-1}), while 2.4 lm W^{-1} (3.4 cd A^{-1}) for the host **6** containing counterpart. The reason why the host **5** containing device exhibited highest efficiencies amongst all the three studied hosts may be attributed to three efficiency effective device architecture approaches, which are i) feasibility of effective exciton generation on both host and guest, ii) high triplet energy, and iii) effective host-to-guest energy transfer.

As shown in **Fig. 3**, the hole injection barrier for host **5** is 0.34 eV, which is lower than that (0.36 eV) of the green $Ir(ppy)_3$ emitter, enabling more holes to transport to host **5**. Whilst, the same architecture favors the injection of electrons into the guest because there exists a -0.3 eV electron trap, in contrast to a 0.81 eV barrier to enter into the host. These would hence lead excitons to generate on both host and guest and result in high device efficiency.[10, 31-33]

Furthermore, the hosts **4** and **5** showed a triplet-energy of 2.57 eV, higher than that of the green emitter, whose triplet-energy is 2.57 eV.[34,35] This would allow the hosts

View Article Online
DOI: 10.1039/C5TC02889B

4 and **5** to enable an effective host-to-guest energy transfer and exciton confinement on guest, resulting in high device efficiency.[36-38] In contrast, the host **6** showed a slightly lower triplet energy of 2.47 eV, which is not able to prevent the back energy transfer from guest to host.[10,33,39]

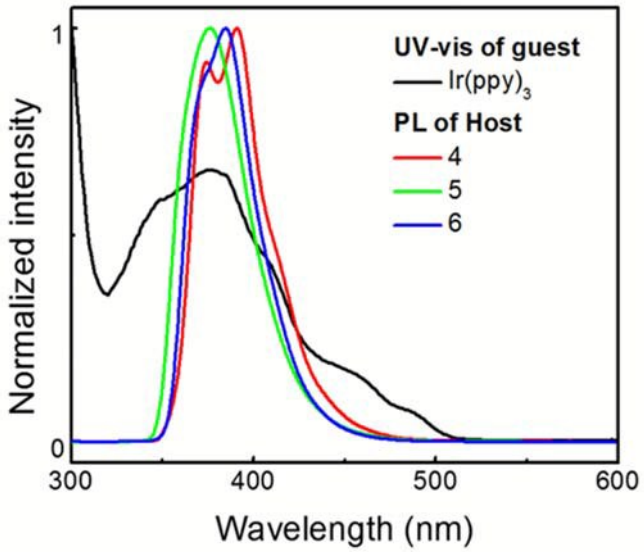

Figure 5. The corresponding overlapping between the PL spectra of the hosts **4**, **5**, and **6** with the UV-vis spectrum of the $Ir(ppy)_3$ dopant.

As shown in **Fig. 5**, all the three host materials can effectively transfer their energy to the green emitter, as indicated by the large overlapping area between the PL spectra of the hosts **4**, **5**, and **6** and the UV-vis spectrum of the guest. However, host **5** showed a PL emission peaking at a wavelength (376 nm) much lower than that of the hosts **4** (391 nm) and **6** (385 nm), which would trigger the higher energy emission of the guest, leading to a higher device efficiency.[40]

View Article Online
DOI: 10.1039/C5TC02889B

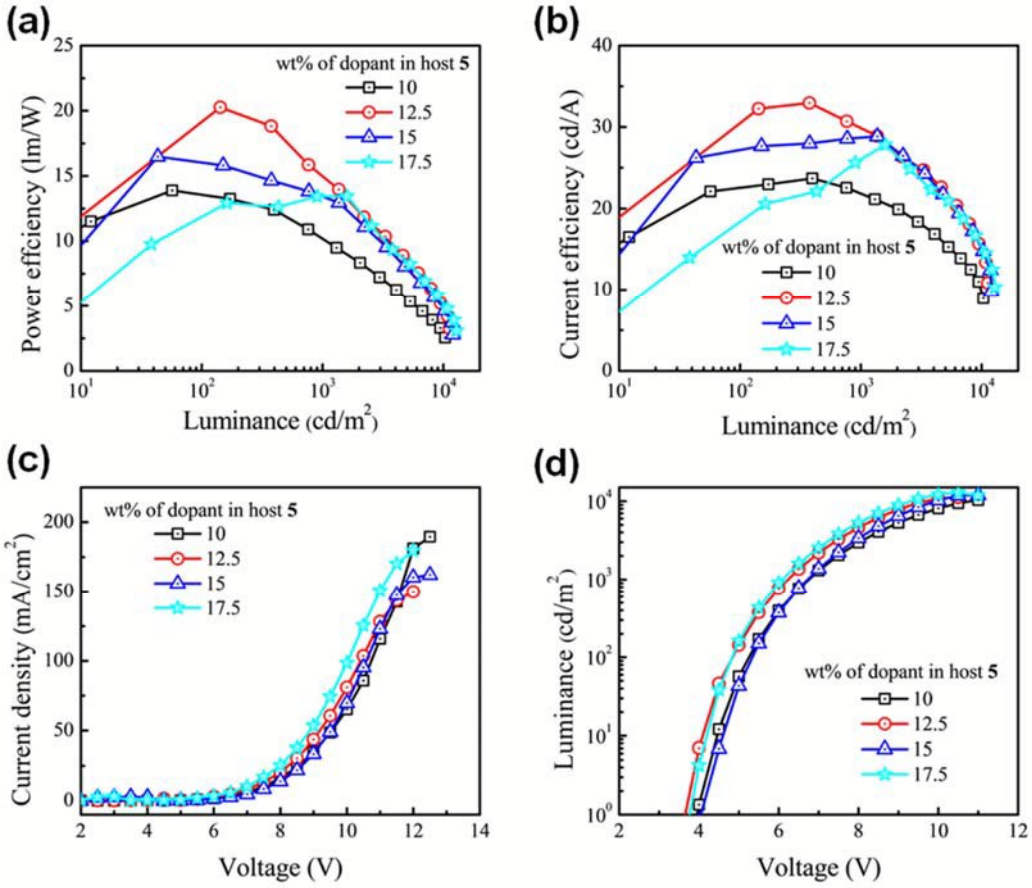

Figure 6. Doping concentration effects on the a) power efficiency, b) current efficiency, c) current density, and d) luminance results of the host **5** based green OLED devices.

As shown in **Fig. 6**, the device efficiencies significantly depend on the doping concentration of the green emitter. Taking the host **5** based device for example, the power efficiency at 100 cd m^{-2} increased from 13.1 to 16.1 lm w^{-1} as doping concentration was increased from 10 to 15 wt%. However, as the concentration further increased to 17.5%, the efficacy decreased to 11.3 lm W^{-1}. This may be attributed to the triplet-triplet annihilation as well as concentration-quenching, resulted from self-aggregation of the emitter at high concentration.[10,17,18] Moreover, as the doping

View Article Online
DOI: 10.1039/C5TC02889B

concentration increases from 10 to 15 wt% the electroluminescence (EL) spectra exhibit a stable emission peak at 516 nm. When the doping concentration is further increased to 17.5 wt%, a bathochromic shift is observed with emission peaking at 520 nm. However, as the concentration is increased to 17.5 wt%, the efficiencies start to drop. This may be attributed to a concentration-quenching effect that can be confirmed by a 4 nm bathochromic shift in the EL spectrum of the 17.5 wt% $Ir(ppy)_3$ doped host **5** based device, as shown in **Fig.7**.[17,18,41]

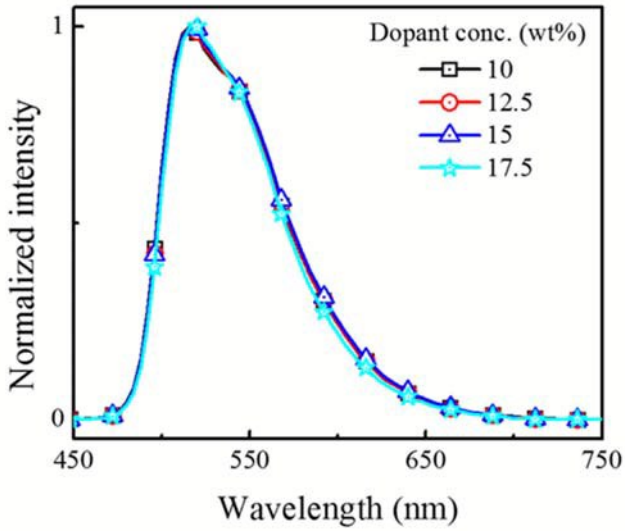

Figure 7. Effect of dopant concentration on the electroluminescence (EL) spectra of the device containing host **5**. The EL emission spectra becomes slightly narrower as the dopant concentration was increased from 15 to 17.5 wt%, while the spectra remain unchanged as the dopant concentration was changed from 10 to 15 wt%.

Table 3. Effect of host materials on the turn-on voltage (V_{ON}), operation voltage (OV), power efficiency (PE), current efficiency (CE), external quantum efficiency (EQE), CIE coordinates, and maximum luminance of the hosts (**4**, **5**, and **6**) doped with 10 wt% $Ir(ppy)_3$ green emitter based dry-processed OLED devices.

Host	ECL	V_{ON} (V)	OV (V)	PE (lm/W)	CE (cd/A)	EQE (%)	CIE coordinates	Max. Luminance (cd/m^2)
		@ 10 cd/m^2	@ 100/1000 cd/m^2					
4	-	2.9	3.2/ 3.9	16.9/ 17.3	17.3/ 21.3	4.7/ 5.8	(0.32, 0.62)/ (0.32, 0.62)	25810
	TAPC	2.7	3.1/ 3.7	42.9/ 30.7	41.8/ 36.3	11.7/ 10.2	(0.31, 0.62)/ (0.31, 0.62)	26070
5	-	3.1	3.5/ 4.1	52.7/ 42.7	59.4/ 55.3	16.4/ 15.3	(0.31, 0.63)/ (0.3, 0.63)	36810
	TAPC	2.6	3.1/ 3.7	62.8/ 47.4	61/ 55.4	17.2/ 15.7	(0.33, 0.61)/ (0.33, 0.61)	47890
6	-	4.0	4.6/ 5.9	3.1/ 1.5	4.5/ 2.8	2.2/ 1.7	(0.23, 0.4)/ (0.22, 0.33)	2181
	TAPC	3.1	3.8/ 6.0	7.9/ 3.4	9.5/ 6.4	3.3/2.6	(0.25, 0.47)/ (0.24, 0.41)	3964

View Article Online
DOI: 10.1039/C5TC02889B

2.5.2 Dry processed devices

The efficiency performance of the new synthesized host materials is further investigated via vapor evaporation deposition. **Table 3** shows the electroluminescent characteristics of the thermal evaporation based OLED devices containing hosts **4**, **5**, and **6** doped with a 10 wt% $Ir(ppy)_3$ green emitter. The resultant host **5** containing device is also better than that of the host **4** and **6** containing counterparts. At 100 cd m^{-2} for example, host **5** based device exhibits a power efficiency of 52.7 lm W^{-1} and a current efficiency of 59.4 cd A^{-1} with a maximum luminance of 36,810 cd m^{-2}, respectively, which are over 200%, 240%, and 40% higher than that of host **4** containing counterpart. These results are also significantly higher than that of spin-coated EML based devices. The reason why the dry-processed devices showed better performance may be due to better film uniformity and integrity, while pin-holes and rougher surface might easily present in the resultant films from wet process especially after the evaporation of the solvent applied.

The host **4** containing device showed higher device efficiencies than that of the host **6**. Taking 100 cd m^{-2} for example, host **6** based device exhibited a power efficiency of 3.1 lm W^{-1} and a current efficiency of 4.5 cd A^{-1}, which are nearly 450% and 280%, respectively, lower than the host **4** based device. When host **6** was used as host, both holes and electrons prefer to enter into the guest rather than into the host, because the respective barrier for holes to emitter is 0.11 eV lower than that of the host. The $Ir(ppy)_3$

View Article Online
DOI: 10.1039/C5TC02889B

guest possesses an effective electron injection pathway, i.e., it shows a -0.3 eV electron trap, in contrast to the host **6** that has an electron injection barrier of 0.39 eV. As a result, the majority of the excitons would form on the $Ir(ppy)_3$ guest, which could not trigger the higher energy emission. Moreover, the reason why the host **6** based device exhibits such poor efficiencies may be attributed to its low triplet energy.[10,33,39]

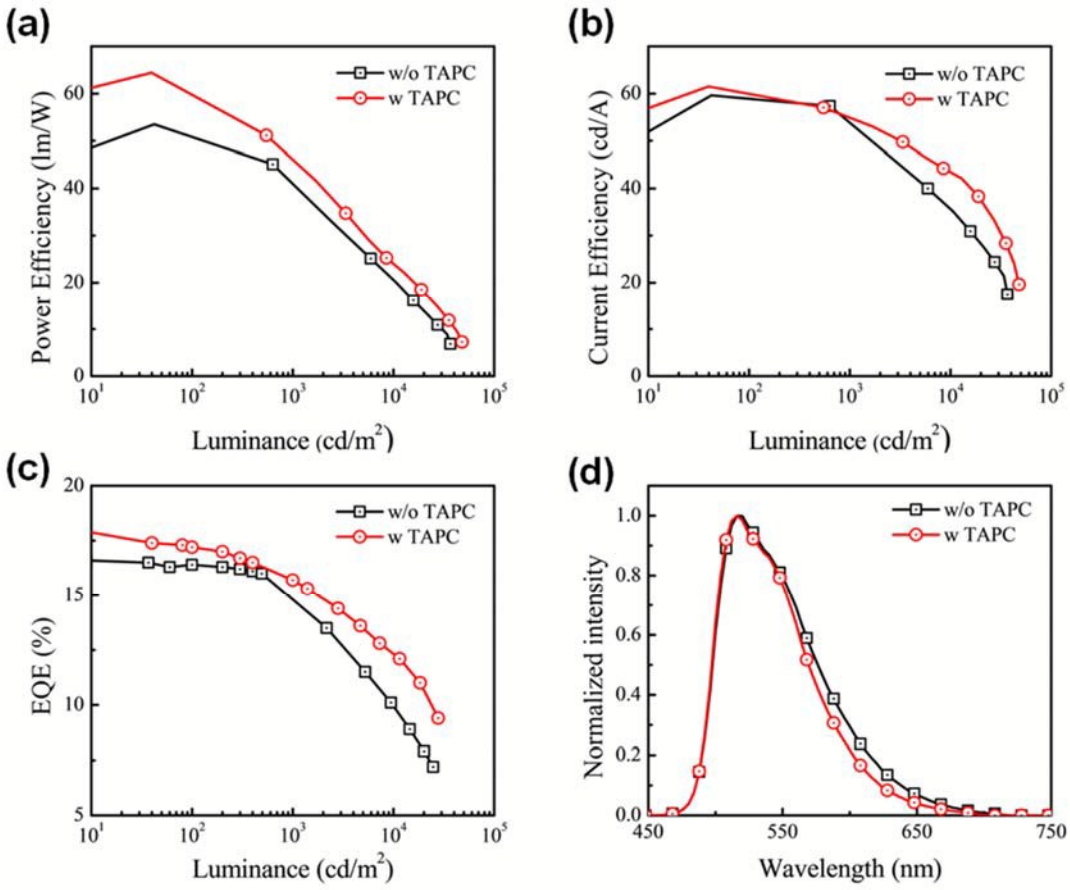

Figure 8. Effect of hole transporting layer, TAPC, on the **a)** luminance, **b)** power efficiency, **c)** current efficiency, and **d)** EQE results of the devices with 10 wt% $Ir(ppy)_3$ green emitter doped into the host **5**.

The device efficiency was further enhanced as a 20 nm hole transporting layer, TAPC, was deposited between the PEDOT:PSS layer and EML. As shown in **Fig. 8**,

View Article Online
DOI: 10.1039/C5TC02889B

for the host **5** containing device, the resultant power efficiency, current efficiency, and EQE were increased from 52.7 to 62.8 lm W^{-1}, 59.4 to 61 cd A^{-1}, and 16.4 to 17.2%, respectively. By comparing the without TAPC (w/o TAPC) device, a narrow EL spectrum is observed for the TAPC based device (w TAPC) counterpart, which may result because of a small shift in the recombination zone. Moreover, the resultant device also exhibited a significant enhancement in luminance, which increased from 36,810 to 47,890 cd/m^2. For the host **4** containing device, the resultant power efficiency, current efficiency, and EQE was increased from 16.9 to 42.9 lm W^{-1}, 17.3 to 41.8 cd A^{-1}, and 4.7 to 11.7%, respectively, while 3.1 to 7.9 lm W^{-1}, 4.5 to 9.5 cd A^{-1}, and 2.2 to 3.3%, for the host **6**-containing counterpart (**Table 3**). This enhancement may be attributed to the fact that TAPC possesses an electron-modulating function.[42,43] As shown in **Fig. 3(b)**, the HOMO level of TAPC is 0.6 eV lower than that of PEDOT, which may block a certain number of holes from entering the emissive-layer, balancing the carrier-injection and improving the device efficiency.[44,45]

3. Conclusion

To conclude, in this report we demonstrate a new carbazole-based host **5** with both wet- and dry-process feasibility. By employing this host, green phosphorescent OLED devices with higher efficiencies have been fabricated. The device shows, at 100 cd m^{-2} for example, a power efficiency of 16.1 lm W^{-1} (27 cd A^{-1}) by using spin-coating, while

View Article Online
DOI: 10.1039/C5TC02889B

52.7 lm W^{-1} (59.4 cd A^{-1}) using vapor-deposition. The high efficiency may be attributed to feasibility of effective exciton generation on both host and guest, high triplet energy, and effective host-to-guest energy transfer. The device efficiencies can be further enhanced to 62.8 lm W^{-1} (61 cd A^{-1}) by incorporating a TAPC hole transporting layer. The resultant carbazole derivative may serve as one ideal host for fabricating energy-efficient devices for solid state lighting and flat panel display applications via either wet- or dry-processing.

4. Experimental

4.1 Synthesis

1,6-Bis[3-(6-methoxy-3-pyridinyl)carbazol-9-yl]hexane (**4**) 1.2 g (1.8 mmol) of 1,6-bis(3-iodocarbazol-9-yl)hexane (**3**), 0.8 g (5.4 mmol) of 6-methoxy-3-pyridinylboronic acid, 0.05 g (0.08 mmol) of $PdCl_2(PPh_3)_2$ and 0.5 g (8.5 mmol) of powdered potassium hydroxide were stirred in 20 ml of THF containing degassed water (2 ml) at 80 °C under nitrogen for 24 h. After TLC control the reaction mixture was cooled and quenched by the addition of ice water. The product was extracted by ethyl acetate. The combined extract was dried over anhydrous Na_2SO_4. The crude product was purified by silica gel column chromatography using the mixture of ethyl acetate and hexane (vol. ratio 1:5) as an eluent. Yield: 0.79 g of yellow crystals.

MS ($APCI^+$, 20 V): 631.3 ([M+H], 100 %). ^1H NMR (300 MHz, $CDCl_3$, δ, ppm): 8.38 (d, 2H, *J*=2.7Hz, Ar), 8.12 (d, 2H, *J*=1.5Hz, Ar), 8.03 (d, 2H, *J*=7.5Hz, Ar), 7.80 (dd,

View Article Online
DOI: 10.1039/C5TC02889B

2H, J_1=2.4Hz, J_2=8.7Hz Ar), 7.47 (dd, 2H, J_1=1.95Hz, J_2=8.4Hz Ar), 7.39-7.11 (m, 6H, Ar), 6.76(d, 2H, J=8.4Hz, Ar), 4.17 (t, 4H, J=6.9Hz, $N\underline{CH_2}(CH_2)_4\underline{CH_2}N$), 3.92(s, 6H, $2\times O\underline{CH_3}$), 1.78-1.68(m, 4H, $NCH_2\underline{CH_2}(CH_2)_2\underline{CH_2}CH_2N$), 1.35-1.31(m, 4H, $NCH_2CH_2(\underline{CH_2})_2CH_2CH_2N$). ^{13}C NMR ($CDCl_3$, δ, ppm): 162.98, 144.78, 140.80, 139.80, 137.82, 131.10, 125.97, 124.67, 123.44, 122.75, 120.46, 119.05, 118.47, 110.72, 109.04, 108.79, 53.61, 42.93, 28.84, 27.05.

1,6-Bis[3-(2-methoxy-3-pyridinyl)carbazol-9-yl]hexane (**5**) 1.6 g (2.4 mmol) of 1,6-bis(3-iodocarbazol-9-yl)hexane (**3**), 0.9 g (6.01 mmol) of 2-methoxy-3-pyridinylboronic acid, 0.07 g (0.10 mmol) of $PdCl_2(PPh_3)_2$ and 0.7 g (12.5 mmol) of powdered potassium hydroxide were stirred in 20 ml of THF containing degassed water (2 ml) at 80 °C under nitrogen for 24 h. After TLC control the reaction mixture was cooled and quenched by the addition of ice water. The product was extracted by ethyl acetate. The combined extract was dried over anhydrous Na_2SO_4. The crude product was purified by silica gel column chromatography using the mixture of ethyl acetate and hexane (vol. ratio 1:5) as an eluent. Yield: 0.76 g of amorphous material.

MS (APCI$^+$, 20 V): 631.3 ([M+H], 100 %). ^{1}H NMR (300 MHz, $CDCl_3$, δ, ppm): 8.27(d, 2H, J=1.8Hz, Ar), 8.17 (dd, 2H, J_1=1.95Hz, J_2=5.1Hz, Ar), 8.12 (d, 2H, J=7.2Hz, Ar), 7.71(dd, 2H, J_1=1.5Hz, J_2=7.2Hz, Ar), 7.65 (dd, 2H, J_1=1.65Hz, J_2=8.7Hz, Ar), 7.49-7.33 (m, 6H, Ar), 7.27-7.20 (m, 2H, Ar), 7.00 (dd, 2H, J_1=1.95Hz, J_2=5.1Hz, Ar), 4.28 (t, 4H, J=7.35Hz, $N\underline{CH_2}(CH_2)_4\underline{CH_2}N$), 4.01 (s, 6H, $2\times O\underline{CH_3}$), 1.95-1.82 (m, 4H, $NCH_2\underline{CH_2}(CH_2)_2\underline{CH_2}CH_2N$), 1.43-1.39 (m, 4H, $NCH_2CH_2(\underline{CH_2})_2CH_2CH_2N$). ^{13}C NMR ($CDCl_3$, δ, ppm): 161.05, 144.96, 104.74, 139.79, 138.74, 127.37, 127.01, 125.75, 125.55, 122.87, 121.08, 120.44, 118.94, 117.16, 108.69, 108.28, 53.55, 42.89, 28.85, 27.05.

3,6-Di(2-methoxy-3-pyridinyl)-9-ethylcarbazole (**6**) 2.0 g (4.47 mmol) of 3,6-diiodo-9-ethylcarbazole (**DECr**), 1.5 g (9.8 mmol) of 2-methoxy-3-pyridinylboronic acid, 0.037 g (0.14 mmol) of $PdCl_2(PPh_3)_2$ and 1 g (17.8 mmol) of powdered potassium

View Article Online
DOI: 10.1039/C5TC02889B

hydroxide were stirred in 20 ml of THF containing degassed water (1.5 ml) at 80 °C under nitrogen for 24 h. After TLC control the reaction mixture was cooled and quenched by the addition of ice water. The product was extracted by ethyl acetate. The combined extract was dried over anhydrous Na_2SO_4. The crude product was purified by silica gel column chromatography using the mixture of ethyl acetate and hexane (vol. ratio 1:5) as an eluent. Yield: 1.25 g of yellow crystals. M.p.: 137 ºC (DSC).

MS (APCI$^+$, 20 V): 424.1 ([M+H], 100 %). ^{1}H NMR (300 MHz, $CDCl_3$, δ, ppm): 8.28 (d, 2H, *J*=0.9Hz, Ar), 8.16 (dd, 2H, J_1=1.5Hz, J_2=1.8Hz, Ar), 7,74 (d, 1H, *J*=1.5Hz, Ar), 7.73-7.70(m, 2H, Ar),7.68 (d, 1H, *J*=1.2Hz, Ar), 7.47 (d, 2H, *J*=6.3Hz, Ar), 7.03-6.99(m, 2H, Ar), 4.42(q, 2H, *J*=7.2Hz, N$\underline{CH_2}CH_3$), 4.01(s, 6H, 2×O$\underline{CH_3}$), 1.48(tr, 3H, *J*=7.2Hz, $NCH_2\underline{CH_3}$). ^{13}C NMR ($CDCl_3$, δ, ppm): 161.08, 144.99, 139.77, 138.76, 127.56, 127.17, 125.56, 123.09, 121.25, 117.17, 108.26, 53.58, 37.74, 13.93.

4.2 *Materials*

9*H*-Carbazole (1), 6-methoxy-3-pyridinylboronic acid, 2-methoxy-3-pyridinylboronic acid, 1,6-dibromohexane, tetra-*N*-butylammonium hydrogen sulphate (TBAHS), tetra-n-butyl ammonium chloride, potassium iodide, potassium iodate, bis(triphenylphosphine)palladium(II) dichloride ($Pd(PPh_3)_2Cl_2$), Alq_3, sodium hydroxide and potassium hydroxide were purchased from Aldrich and used as received. All the precursor compounds required for the synthesis were used as such without further purification. 3-Iodo-9*H*-carbazole (**2**) was obtained by a procedure of Tucker.[21] 1,6-Bis[3-iodocarbazol-9-yl]hexane (**3**) was synthesized by using the prior

View Article Online
DOI: 10.1039/C5TC02889B

methodology.[22]

The indium tin oxide (ITO) coated glass substrates with sheet resistance of 15 Ω/□ and light transmittance greater than 84% were purchased from Luminescence Technology Corporation. The hole injection material poly(3,4-ethylene-dioxythiophene)-poly(styrenesulfonate) (PEDOT:PSS) with purity of 99.9% was purchased from Bayer Taiwan Company. The electron confining/hole transporting materials di-[4-(*N,N*-ditolylamino)-phenyl]cyclohexane (TAPC), and an electron transporting material 1,3,5-tris(*N*-phenylbenzimidazol-2-yl)benzene (TPBi) were purchased from e-Ray optoelectronic co. ltd. A typical green emitter tris(2-phenyl-pyridine) iridium ($Ir(ppy)_3$ was purchased from Luminescence Technology Corporation. Lithium fluoride (LiF) (purity 99.95%) was purchased from Strem Chemicals Corporation. Aluminum (Al) ingots (99.999%) were purchased from Showa Chemical Co. Ltd. All materials were used without further purification.

4.3 Characterizations and measurements

Column chromatography purifications were performed with silica gel (70-230 mesh) as a stationary phase in a column with 50 cm long and 5 cm diameter. ^{1}H NMR spectra were recorded using a Varian Unity Inova (300 MHz) apparatus. Mass spectra of the compounds were obtained on a Waters ZQ 2000 spectrometer in the positive ion mode. The PL spectra were recorded in THF at room temperature in quartz cuvettes using a

View Article Online
DOI: 10.1039/C5TC02889B

Fluorolog III photoluminescence spectrometer. UV-vis spectra were also recorded in THF at room temperature using a UV-Visible spectrophotometer.

Cyclic voltammetry (CV) experiments were performed on an electrochemical workstation using a three electrode assembly comprising glassy carbon working electrode, a non-aqueous Ag/AgCl reference electrode and an auxiliary platinum electrode. The experiments were performed at room temperature under nitrogen atmosphere in dichloromethane using 0.1 M tetrabutylammonium perchlorate (Bu_4NClO_4) as supporting electrolyte on a Chinstruments CH1604A potentiostat. The $E_{1/2}^{ox}$ values were determined as $(E_p^a + E_p^c)/2$, where E_p^a and E_p^c are the anodic and cathodic peak potentials, respectively.

Differential scanning calorimetry (DSC) measurements were carried out using a Bruker Reflex II thermosystem. Thermogravimetric analysis (TGA) was performed on a Netzsch STA 409. TGA and DSC curves were recorded in a nitrogen atmosphere at a heating rate of 10 $^oC\ min^{-1}$.

4.4 Device fabrication and characterization

4.4.1 Wet-processed

Fig. 3 (a) shows the schematic energy-level diagram of green OLEDs studied herein. The fabrication process included firstly spin-coating an aqueous solution of PEDOT:PSS at 4,000 rpm for 20 s to form a hole-injection layer (HIL) on a pre-cleaned

View Article Online
DOI: 10.1039/C5TC02889B

ITO anode. Before depositing the following emissive layer, the solution was prepared by dissolving the $Ir(ppy)_3$ guest in three different novel host materials, 4, 5 and 6, in THF at room-temperature for 0.5 h with stirring. The resulting solution was then spin-coated at 2,500 rpm for 20 s under nitrogen. Followed were the depositions of an electron-transporting layer TPBi, an electron injection layer LiF, and a cathode Al, by thermal evaporation in a vacuum chamber at the vacuum level of less than 5×10^{-6} Torr.

4.4.2 Dry-processed

In a dry-processed OLED devices (**Fig. 3 (a)** and **(b)**), a 32 nm HIL of PEDOT:PSS was spin coated on a pre-cleaned ITO anode. Subsequently, an optional 20 nm hole transporting layer (HTL) of TAPC, a 20 nm EML, a 35 nm ETL of TPBi, a 1 nm EIL of LiF, and a 100 nm Al cathode, were deposited by thermal evaporation in a vacuum chamber at the ultra-high vacuum condition. The dry-process EML source was prepared by the solution pre-mixing[46] of the $Ir(ppy)_3$ guest in the three different host materials, **4**, **5**, and **6**.

4.4.3 Characterization

The luminance, CIE chromatic coordinates, and electroluminescent spectrum of the resultant green OLEDs were measured by using Photo Research PR-655 spectrascan. Keithley 2400 electrometer was used to measure the current-voltage (I–V) characteristics. The emission area of the devices was 25 mm^2, and only the luminance

View Article Online
DOI: 10.1039/C5TC02889B

in the forward direction was measured.

Acknowledgements

This work was financially supported by Ministry of Science and Technology through the grant numbers of 104-2119-M-007 -012- and 103-2923-E-007 -003 -MY3, Ministry of Economic Affairs through the grant number MEA 102-EC-17-A-07-S1-181 and by Research Council of Lithuania through the grant number of TAPLLT1/2014.

References

1. F. So, J. Kido and P. Burrows, *MRS Bull.*, 2008, **33**, 663.
2. (a) S. R. Forrest, *Nature*, 2004, **428**, 911; (b) S. Reineke, M. Thomschke, B. Lüssem and K. Leo, *Rev. Mod. Phys.*, 2013, **85**, 1245.
3. M. A. Baldo, D. F. O'Brien, Y. You, A. Shoustikov, S. Sibley, M. E. Thompson and S. R. Forrest, *Nature*, 1998, **395**, 151.
4. C. Adachi, M. A. Baldo and S. R. Forrest, *Appl. Phys. Lett.*, 2000, **77**, 904.
5. J. P. Duan, P. P. Sun and C. H. Cheng, *Adv. Mater.*, 2003, **15**, 224.
6. Q. Zhang, Q. Zhou, Y. Cheng, L. Wang, D. Ma and X. Jing, *Adv. Mater.*, 2004, **16**, 432.
7. S.-J. Yeh, M.-F. Wu, C.-T. Chen, Y.-H. Song, Y. Chi, M.-H. Ho, S.-F. Hsu and C.-H. Chen, *Adv. Mater.*, 2005, **17**, 285.
8. J. H. Jou, C. H. Chen, J. R. Tseng, S. H. Peng, P. W. Chen, C. I. Chiang, Y. C. Jou, J. H. Hong, C. C. Wang, C. C. Chen, F. C. Tung, S. H. Chen, Y. S. Wang and C. L. Chin, *J. Mater. Chem. C*, 2013, **1**, 394.

View Article Online
DOI: 10.1039/C5TC02889B

9. J. H. Jou, S. H. Peng, C. I. Chiang, Y. L. Chen, Y. X. Lin, Y. C. Jou, C. H. Chen, C. J. Li, W. B. Wang, S. M. Shen, S. Z. Chen, M. K. Wei, Y. S. Sun, H. W. Hung, M. C. Liu, Y. P. Lin, J. Y. Li and C. W. Wang, *J. Mater. Chem. C*, 2013, **1**, 1680.
10. J. H. Jou, S. Kumar, D. Tavgeniene, C. C. An, P. H. Fang, E. Zaleckas, J. V. Grazuleviciusb and S. Grigalevicius, *J. Mater. Chem. C*, 2014, **2**, 8707.
11. Y. Tao, Q. Wang, C. Yang, Q. Wang, Z. Zhang, T. Zou, J. Qin, and D. Ma, *Angew. Chem.*, 2008, **120**, 8224 .
12. H. F. Chen, S. J. Yang, Z. H. Tsai, W. Y. Hung, T. C. Wanga and K. T. Wong, *J. Mater. Chem.*, 2009, **19**, 8112.
13. H. H. Chou and C. H. Cheng, *Adv. Mater.*, 2010, **22**, 2468.
14. J. S. Chen, C. S. Shi, Q. Fu, F. C. Zhao, Y. Hu, Y. L. Feng and D. G. Ma, *J. Mater. Chem.*, 2012, 22, 5164.
15. T.-W. Lee, T. Noh, H.-W. Shin, O. Kwon, J.-J. Park, B.-K. Choi, M.-S. Kim, D. W. Shin and Y.-R. Kim, *Adv. Mater.*, 2009, 19, 1625.
16. J.-H. Jou, C.-J. Li, S.-M. Shen, S.-H. Peng, Y.-L. Chen, Y.-C. Jou, J. H. Hong, C.-L. Chin, J.-J. Shyue, S.-P. Chen, J.-Y. Li, P.-H. Wang and C.-C. Chen, *J. Mater. Chem. C*, 2013, 1, 4201.
17. J. H. Jou, Y. M. Yang, S. Z. Chen, J. R. Tseng, S. H. Peng, C. Y. Hsieh, Y. X. Lin, C. L. Chin, J. J. Shyue, S. S. Sun, C. T. Chen, C. W. Wang, C. C. Chen, S. H. Lai, and F. C. Tung, *Adv. Optical Mater.*, 2013, **1**, 657.
18. J. H. Jou, Y. X. Lin, S. H. Peng, C. J. Li , Y. M. Yang, C. L. Chin, J. J. Shyue, S. S. Sun, M. Lee, C. T. Chen, M. C. Liu, C. C. Chen, G. Y. Chen , J. H. Wu, C. H. Li, C. F. Sung, M. J. Lee, and J. P. Hu, *Adv. Funct. Mater.*, 2014, **24**, 555.
19. J. H. Jou, M. F. Hsu, W. B. Wang, C. L. Chin, Y. C. Chung, C. T. Chen, J. J. Shyue, S. Ming Shen, M. H. Wu, W. C. Chang, C. P. Liu, S. Z. Chen, and H. Y. Chen, *Chem. Mater.*, 2009, **21**, 2565.

View Article Online
DOI: 10.1039/C5TC02889B

20. S. Lengvinaite, J. V. Grazulevicius, S. Grigalevicius, B. Zhang and Z. Xie, *React. Funct. Polym.,* 2010, **70**, 477.

21. S. H. Tucker, *J. Chem. Soc.*, 1926, **1**, 548.

22. S. Grigalevicius, L. Ma, G. Qian, Z. Xie, M. Forster and U. Scherf, *Macromol. Chem. Phys.*, 2007, **208**, 349.

23. a) C.-Q. Ma, M. Fonrodona, M. C. Schikora, M. M. Wienk, R. A. J. Janssen, P. Baeuerle, *Adv. Funct. Mater.*, 2008, 18, 3323. b) R. S. K. Kishore, O. Kel, N. Banerji, D. Emery, G. Bollot, J. Mareda, A. G. Casado, P. Jonkheijm, J. Huskens, P. Maroni, M. Bokovec, E. Vauthey, N. Sakai, S. Matile, *J. Am. Chem. Soc.*, 2009, 131. c) N. F. Montcada, R. Dominguez, B. Pelado, P. de la Cruz, E. Palomares, F. Langa, *J. Mater. Chem. A*, 2015, **3**, 11340.

24. C. A. Amorim, M. R. Cavallari, G. Santos, F. J. Fonseca, A. M. Andrade and S. Mergulhao, *J. Non-Cryst. Solids*, 2012, **358**, 484.

25. S. C. Tse, C. H. Cheung and S. K. So, in: F. So (Ed.), *Taylor & Francis, London*, 2010, **Chapter 3**, 71.

26. W. Y. Hung, L. C. Chi, W. J. Chen, Y. M. Chen, S. H. Chou and K. T. Wong, *J. Mater. Chem.*, 2010, **20**, 10113.

27. M. H. Tsai, T. H. Ke, H. W. Lin, C. C. Wu, S. F. Chiu, F. C. Fang, Y. L. Liao, K. T. Wong, Y. H. Chen and C. I. Wu, *ACS Appl. Mater. Interfaces*, 2009, **1**, 567.

28. J. Ficker, A. Ullmann, W. Fix, H. Rost, W. Clemens, *J. Appl.Phys.* 2003, **94**, 2638.

29. K. L. Woon, Z. A. Hasan, B. K. Ong, A. Ariffin, R. Griniene, S. Grigalevicius, S.-A. Chen, *RSC Adv.*, 2015, 5, 59960.

30. R. R. Lunt, N. C. Giebink, A. A. Belak, J. B. Benziger, S. R. Forrest, *J. Appl. Phys.* 2009, **105**, 053711.

31. J. H. Jou, S. Z. Chen, C. C. An, S. H. Peng, T. Y. Ting, J. J. Shyue, C. L. Chin, C. T. Chen and C. W. Wang, *Dyes Pigments*, 2015, **113**, 341.

View Article Online
DOI: 10.1039/C5TC02889B

32. J.-H. Jou, S. Kumar, A. Agrawal, T.-H. Lee, S. Sahoo, *J. Mater. Chem. C*, 2015, **3**, 2974.

33. J. H. Jou, Y. S. Wang, C. H. Lin, S. M. Shen, P. C. Chen, M. C. Tang, Y. Wei, F. Y. Tsai and C. T. Chen, *J. Mater. Chem.*, 2011, **21**, 12613.

34. N. Li, S.-L. Lai, W. Liu, P. Wang, J. You, C.-S. Lee and Z. Liu, *J. Mater. Chem.*, 2011, **21**, 12977.

35. X. Yang, D. Neher, D. Hertel and T. K. Daubler, *Adv. Mater.*, 2004, **16**, 161.

36. (a) A. P. Kulkarni, C. J. Tonzola, A. Babel and S. A. Jenekhe, *Chem. Mater.*, 2004, **16**, 4556; (b) G. Hughes and M. R. Bryce, *J. Mater. Chem.*, 2005, **15**, 94.

37. Y. Kawamura, S. Yanagida and S. R. Forrest, *J. Appl. Phys.*, 2002, **92**, 87.

38. P. A. Vecchi, A. B. Padmaperuma, H. Qiao, L. S. Sapochak and P. E. Burrows, *Org. Lett.*, 2006, **8**, 4211.

39. a) D. Zhang, L. Duan, Y. Zhang, M. Cai, D. Zhang, and Y. Qiu, *Light: Science & Applications*, 2015, **4**, e232.; b) Y. Tao, C. Yang and J. Qin, *Chem. Soc. Rev.*, 2011,**40**, 2943. c)

40. X. Hui, F. Jaiser, and D. Neher, in: H. Yersin (Ed.), Wiley-VCH, 2008, **Chapter 6**, 221.

41. a) S. Reineke, K. Walzer, K. Leo , *Phys. Rev. B*, 2007, **75**, 125328 ; b) N. C. Giebink, S. R. Forrest, *Phys. Rev. B*, 2008 , **77** , 235215 ; c) Y. Divayana , X. W. Sun , *Phys. Rev. Lett.*, 2007 , **99** , 143003.

42. J. H. Jou, S. M. Shen, S. H. Chen, M. H. Wu, W. B. Wang, H. C. Wang, C. R. Lin, Y. C. Chou, P. H. Wu and J. J. Shyue, *Appl. Phys. Lett.*, 2010, **96**, 143306.

43. J. H. Jou, M. H. Wu, S. M. Shen, H. C. Wang, S. Z. Chen, S. H. Chen, C. R. Lin, and Y. L. Hsieh, *Appl. Phys. Lett.*, 2009, **95**, 013307.

View Article Online
DOI: 10.1039/C5TC02889B

44. J. H. Jou, C. C. Chen, Y. C. Chung, M. F. Hsu, C. H. Wu, S. M. Shen, M. H. Wu, W. B. Wang, Y. C. Tsai, C. P. Wang, and J. J. Shyue, *Adv. Funct. Mater.,* 2008, **18**, 121.

45. J. H. Jou, M. F. Hsu, W. B. Wang, C. P. Liu, Z. C. Wong, J. J. Shyue, and C. C. Chiang, *Org. Electron.*, 2008, **9**, 291.

46. J. H. Jou, Y. S. Chiu, C. P. Wang, R. Y. Wang and C. Hu, *Appl. Phys. Lett.*, 2006, **88**, 193501.